PERGAMON

Polyhedron 21 (2002) 1031–1041

POLYHEDRON

www.elsevier.com/locate/poly

Steric effects on the stereochemistry of copper complexes of 2,6-bis(pyrazol-1-ylmethyl)pyridines

Caroline L. Foster, Colin A. Kilner, Mark Thornton-Pett, Malcolm A. Halcrow *

School of Chemistry, University of Leeds, Woodhouse Lane, Leeds LS2 9JT, UK

Received 4 December 2001; accepted 25 January 2002

Abstract

The stereochemical preferences of copper complexes of 2,6-bis-(3,5-dimethylpyrazol-1-ylmethyl)pyridine (L^1Me_2) and of 2,6-bis-(phenylpyrazol-1-ylmethyl)pyridine (L^1Ph) have been investigated. The single crystal X-ray structures of $[Cu(OH_2)(L^1Me_2)](BF_4)_2$ and $[CuCl(HOMe)(L^1Me_2)]BF_4$ show near-regular tetragonal geometries with one or two axial solvent and/or BF_4^- ligands. In contrast, $[Cu(OH_2)_2(L^1Ph)](BF_4)_2$ adopts an irregular geometry in the crystal mid-way between square-pyramidal and trigonal-bipyramidal. The single crystal X-ray structure of $[Cu(NCMe)(L^1Me_2)]BF_4$ exhibits a distorted tetrahedral geometries, while $[Cu(L^1Ph)]BF_4$ adopts a T-shaped stereochemistry. By a combination of UV–Vis, EPR and conductivity studies, the solution structures of $[CuCl_2(L)]$, $[CuCl(solv)(L)]BF_4$ and $[Cu(solv)_x(L)](BF_4)_2$ ($L = L^1Me_2$, L^1Ph; solv = H_2O, MeCN; $x = 1$, 2) have, in many cases, been shown to be the same as in the crystalline state. The cyclic voltammograms of $[Cu(OH_2)(L^1Me_2)](BF_4)_2$ and $[Cu(OH_2)_2(L^1Ph)](BF_4)_2$ in MeCN/0.1 M $NBu^n_4BF_4$ exhibit chemically reversible Cu(II/I) couples.

Keywords: Copper complexes; Stereochemistry; X-ray structures; Steric properties

1. Introduction

Much of the biomimetic Cu(II) chemistry that has been published over the past 15 years employs facially or meridionally coordinating *tris*-N-donor ligands as protecting groups [1–4]. These are intended to mimic the $[Cu(II)(his)_3L]^{n+}$ ($L = OH^-$, $n = 1$; $L = OH_2$, $n = 2$) centres found in many Type 2 copper [5,6], and all Type 3 and multi-copper [7], proteins. However, despite their utility in this regard, relatively few systematic studies of the stereochemical preferences of Cu(II) centres using this type of ligand have been carried out. This is an important question since, in contrast to many other biometals, the Cu(II) ion readily adopts a wide range of stereochemistries [8]. This can make its chemistry unpredictable and difficult to study, particularly in the absence of strongly coordinating anions.

This paper describes a crystallographic and spectroscopic investigation of the Cu(I) and Cu(II) chemistries of two ligands, L^1Me_2 and L^1Ph (Scheme 1), in the presence and absence of a coordinating anion. Our results complement data from Manoharan and Mukherjee, who reported several compounds of type $[CuX_2(L^1Me_2)]$ (X^- = halide, pseudohalide, NO_2^- or NO_3^-) while our own work was in progress [9–12], and offer a good example of how the Cu(I) and Cu(II) ions adapt their coordination environments in response to steric crowding from the L^1R protecting group. We are aware of only a few similar studies involving other *tris*-N donor ligands. The most relevant example is L^2R, which Karlin and Réglier have shown to cleanly form tetrahedral $[Cu(solv)(L^2R)]^+$ and tetragonal $[Cu(solv)_2(L^2R)]^{2+}$ (solv = MeCN, H_2O) complexes with weakly coordinating anions like triflate and perchlorate [13]. These stereochemistries resemble the structures exhibited by Type 2 and 3 copper biosites, which has contributed to the utility of L^2R ligands in biomimetic Cu chemistry [3,4]. The complexes of L^3–L^9 with Cu(II) salts of weakly coordinating anions have also been studied by Williams [14], Evans [15], and

* Corresponding author. Tel.: +44-113-343-6506; fax: +44-113-343-6565.

E-mail address: m.a.halcrow@chem.leeds.ac.uk (M.A. Halcrow).

0277-5387/02/$ - see front matter
PII: S0277-5387(02)00872-0

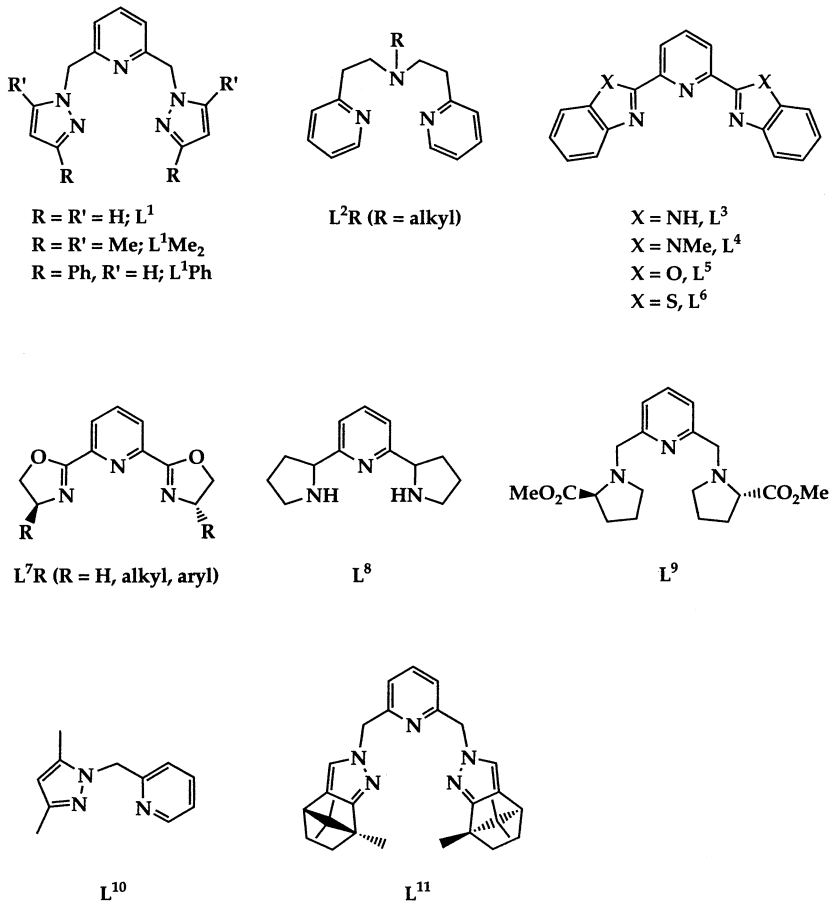

Scheme 1. Ligands referred to in this study.

Bernauer [16]. However, L^3–L^5 and L^7R form helical dimeric complexes with Cu(I) that are not biomimetically relevant [17].

2. Results and discussion

The ligand L^1Me_2 was prepared by the literature method [18], while the new ligand L^1Ph was synthesised in good yield from 3{5}-phenylpyrazole [19] and 2,6-bis-(chloromethyl)pyridine [20], following the literature procedure for L^1 [21].

2.1. Copper(I) complexes of L^1R

Complexation of $[Cu(NCMe)_4]BF_4$ by 1 mole equiv. of L^1Me_2 in MeCN under N_2 gave an air-sensitive yellow solution. Layering of this solution with Et_2O afforded air-stable yellow crystals of $[Cu(NCMe)(L^1Me_2)]BF_4$ (**1**) in low yield, together with a larger amount of unreacted $[Cu(NCMe)_4]BF_4$ which was removed manually. Similar reactions in $MeNO_2$ or CH_2Cl_2 afforded a mixture of **1** and a new pale yellow solid, which we were unable to obtain in analytical purity from this mixture. The FAB mass spectrum of this latter species was identical to that of **1**, while its IR spectrum demonstrated the presence of BF_4^- and L^1Me_2 only. Hence, we tentatively formulate this second complex as solvent-free $[Cu(L^1Me_2)]BF_4$. In contrast to the above reactions, treatment of $[Cu(NCMe)_4]BF_4$ with an equimolar amount of L^1Ph in MeCN, followed by precipitation with Et_2O as before, cleanly afforded the pale yellow air-stable compound $[Cu(L^1Ph)]BF_4$ (**2**).

Single crystals of formula $[Cu(NCMe)(L^1Me_2)]BF_4$ (**1**) and $[Cu(L^1Ph)]BF_4$ (**2**) were grown by layering solutions of the complexes in MeCN and $MeNO_2$, respectively, with Et_2O under N_2. The structure of **1** shows an irregular, distorted tetrahedral geometry at Cu(1) (Fig. 1, Table 1), which is, however, similar to those previously described for $[Cu(PPh_3)(L^1Me_2)]ClO_4$ and $[\{Cu(L^1Me_2)\}_2(\mu\text{-dppe})](ClO_4)_2$ [22]. Of particular interest are the unequal angles N(10)–Cu(1)–N(24) and N(18)–Cu(1)–N(24), and the fact that all four Cu–N bond lengths are significantly different. There are no intramolecular steric contacts that would account for these irregularities. However, the packing diagram of **1** shows there is a close contact between C(26) and F(30′) (symmetry operation $x, -1+y, z$) of 3.352(2) Å, which would appear to prevent the MeCN ligand from occupying its idealised position in the coordination

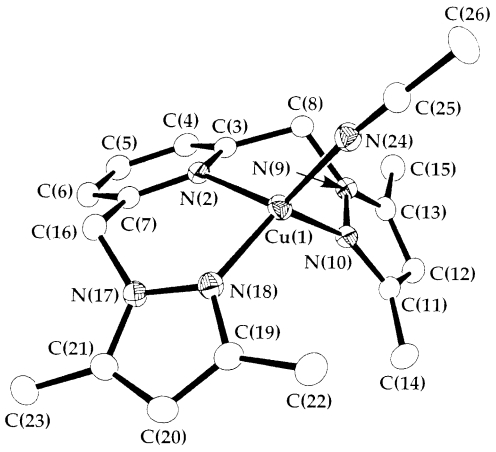

Fig. 1. View of the $[Cu(NCMe)(L^1Me_2)]^+$ complex cation in the structure of **1**, showing the atom numbering scheme employed. Thermal ellipsoids are drawn at the 35% probability level. For clarity, all C-bound H atoms have been omitted.

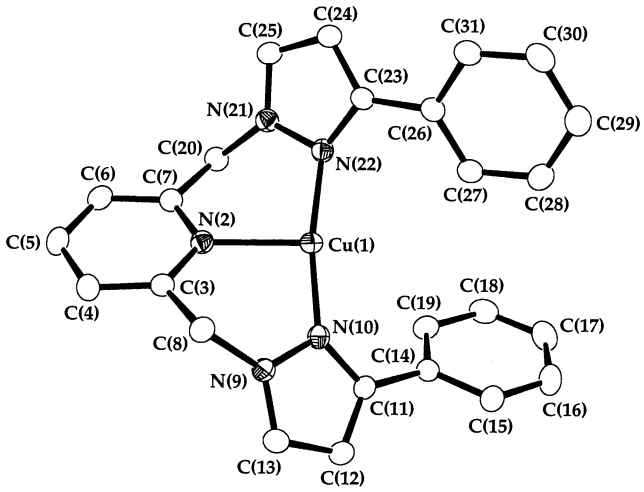

Fig. 2. View of the $[Cu(L^1Ph)]^+$ complex cation in the structure of **2**, showing the atom numbering scheme employed. Details as for Fig. 1.

Table 1
Selected bond lengths (Å) and angles (°) in the single crystal X-ray structures of $[Cu(NCMe)(L^1Me_2)]BF_4$ (**1**) and $[Cu(L^1Ph)]BF_4$ (**2**)

1		**2**	
Bond lengths			
Cu(1)–N(2)	2.1198(12)	Cu(1)–N(2)	2.108(2)
Cu(1)–N(10)	2.1044(13)	Cu(1)–N(10)	1.914(2)
Cu(1)–N(18)	1.9922(13)	Cu(1)–N(22)	1.9175(19)
Cu(1)–N(24)	1.9425(14)		
Bond angles			
N(2)–Cu(1)–N(10)	89.10(5)	N(2)–Cu(1)–N(10)	94.74(8)
N(2)–Cu(1)–N(18)	95.16(5)	N(2)–Cu(1)–N(22)	96.01(8)
N(2)–Cu(1)–N(24)	124.42(6)	N(10)–Cu(1)–N(22)	168.72(8)
N(10)–Cu(1)–N(18)	120.84(5)		
N(10)–Cu(1)–N(24)	103.27(5)		
N(18)–Cu(1)–N(24)	121.04(6)		

sphere. Hence, these molecular distortions can probably be attributed to intermolecular steric contacts.

The complex cation in **2** has a regular T-shaped geometry (Fig. 2, Table 1). The bonds Cu(1)–N(10) and Cu(1)–N(22) are now crystallographically equal, while the angle N(10)–Cu(1)–N(22) has increased to 168.74(8)°, compared with the equivalent angle in **1** of 120.84(5)°. Despite this large variation in *trans*-N–Cu–N angle, the chelate bite angle of the L^1R ligand varies only slightly in the two structures, from an average of 92.14(7)° in **1** to 95.36(11)° in **2**. Rather, these differences reflect differing chelate ring conformations in the structures, which are chair-like in **1** and boat-like in **2**.

2.2. Syntheses and crystal structures of copper(II) complexes of L^1R

Complexation of hydrated $Cu(BF_4)_2$ by an equimolar amount of L^1Me_2 in $MeNO_2$, followed by diffusion of Et_2O into the resultant solution, yielded hygroscopic dark blue microcrystals. Upon prolonged drying in vacuo, these transformed to a blue powder that analysed consistently as $[Cu(OH_2)(L^1Me_2)](BF_4)_2\cdot H_2O$ (**3**·H_2O). Since the crystallographic analysis of this material (see below) showed only 1 mole equiv. of water, it is uncertain whether the second mole of water absorbed by the 'dried' solid is coordinated to the copper ion. A similar reaction employing L^1Ph gave a red–brown crystalline solid $[Cu(OH_2)_2(L^1Ph)](BF_4)_2$ (**4**). Green, sparingly soluble $[CuCl_2(L^1Me_2)]$ (**5**) [9] and $[CuCl_2(L^1Ph)]$ (**6**) were also prepared, by treatment of $CuCl_2$ with the appropriate ligand in MeCN. Reaction of these solids with 1 molar equiv. of $AgBF_4$ in MeCN yielded blue ($L = L^1Me_2$) or green ($L = L^1Ph$) solutions, which were evaporated to dryness. Recrystallisation of the crude materials from MeOH–Et_2O gave $[CuCl(HOMe)(L^1Me_2)]BF_4$ (**7**) and $[CuCl(OH_2)(L^1Ph)]BF_4$ (**8**) as microcrystalline solids.

Single crystals of formula $[Cu(OH_2)(L^1Me_2)](BF_4)_2$ (**3**) and $[CuCl(HOMe)(L^1Me_2)]BF_4$ (**7**) were grown by vapour diffusion from MeOH–Et_2O. Crystals of $[Cu(OH_2)_2(L^1Ph)](BF_4)_2$ (**4**) were similarly obtained from $MeNO_2$–Et_2O. The molecular structures of **3** and **7** are rather similar. Complex **3** contains a near-regular square-planar $[Cu(OH_2)(L^1Me_2)]^{2+}$ centre (Fig. 3, Table 2; structure A in Scheme 2) with a τ index [23] of 0.10, which is very close to the ideal value of 0 for a regular square-pyramid. There are weak axial interactions between Cu(1) and both BF_4^- anions to yield a [4+2] tetragonal Cu(II) ion [Cu(1)···F(26) = 2.531(2), Cu(1)···F(34) = 3.049(3) Å]. Both anions are also involved in hydrogen-bonding to the aqua ligand. One anion interacts with the aqua ligand on the same cation to which it forms an axial interaction. The other (disordered) anion forms hydrogen bonds to a neighbouring cation, yielding a 1-D polymeric lattice composed of alternating Cu···F and F···H–O interactions.

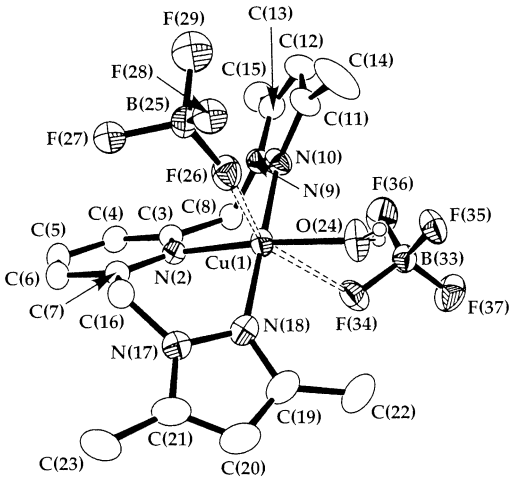

Fig. 3. View of the $[Cu(OH_2)(L^1Me_2)](BF_4)_2$ moiety in the structure of **3**, showing the atom numbering scheme employed. Details as for Fig. 1. For clarity, only one orientation of the disordered BF_4^- anion B(25)–F(29) is shown.

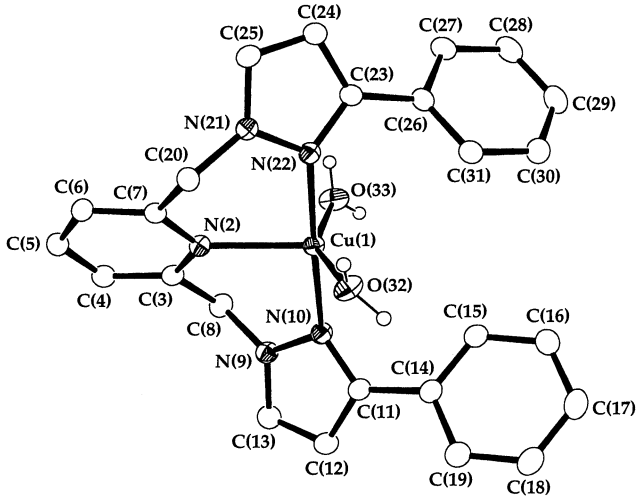

Fig. 4. View of the $[Cu(OH_2)_2(L^1Ph)]^{2+}$ complex dication in the structure of **4**, showing the atom numbering scheme employed. Details as for Fig. 1.

In **7**, the copper ion also adopts structure A (Scheme 2), with an apical MeOH ligand [Cu(1)–O(25) = 2.362(3) Å, $\tau = 0.11$] (Fig. 5, Table 2). The cations in the crystal are arranged into dimers, by hydrogen-bonding between the MeOH hydroxyl proton and a Cl^- ligand of a neighbouring cation related by $1-x, -y, 1-z$.

In contrast to the L^1Me_2 compounds, the copper ion in **4** has an irregular five-coordinate structure, which corresponds to structure B in Scheme 2 (Fig. 4, Table 2). This structure could be considered as trigonal-bipyramidal with the pyrazole N-donors axial [N(10)–Cu(1)–N(22) = 177.84(6)°], or as square-pyramidal with the pyridine N-donor apical [Cu(1)–N(2) = 2.1879(15) Å]. The τ index for this compound is in fact 0.46, almost exactly midway between the limiting values for a regular square-pyramid ($\tau = 0$) or trigonal-bipyramid ($\tau = 1$) [23]. The four protons on the water ligands in **4** are each hydrogen bonded to a different BF_4^- anion, forming a 1-D chain polymer motif in the crystal.

2.3. Conductivity, UV–Vis and EPR measurements

Solution UV–Vis and conductivity data for the Cu(II) compounds in this study, in both MeCN and $MeNO_2$ solutions, are listed in Table 3. Conductivity measurements for all of the Cu(II) complexes in this study were consistent with their solid state molecular structures. Hence, complexes **5** and **6** exhibit molar conductivities consistent with their being non-electrolytes in both these solvents, while **7** and **8** are clearly 1:1 electrolytes and **3** and **4** are 2:1 electrolytes [24]. This demonstrates that Cl^--dissociation does not take place upon dissolution of the chloride-containing complexes in MeCN or $MeNO_2$, which is consistent with an earlier study of **5** in dmf solution [9].

The visible spectra of **3**–**8** each exhibit a single d–d band (Table 3). The d–d spectra of **5**–**7** are essentially identical in MeCN and $MeNO_2$. This shows that they adopt the same molecular structures in these two solvents, and that dissociation of Cl^- or the L^1R ligand does not take place upon dissolution. However, the d–d maximum for **8** lies at a slightly lower wavelength in $MeNO_2$ than in MeCN. This suggests that, although the coordination geometry of **8** probably does not vary between the two solvents, solvent coordination is more important to the solution structure of **8** than **7**. Unsurprisingly, the d–d maxima of **3** and **4** are very solvent dependent. For **3**, **4** and **8**, the d–d maxima lie at longer wavelength in MeCN than in $MeNO_2$, which is consistent with the relative positions in the spectrochemical series of MeCN and H_2O [25] (the probable 'solv' ligand in $MeNO_2$, since $MeNO_2$ itself is an extremely poor ligand [26]).

As solids, the X-band EPR spectra of **4**–**6** and **8** are well-resolved into a clearly rhombic pattern, the g-values for each of these compounds being quite similar (Table 4). We, therefore, propose that **6** and **8** adopt structure B (Scheme 2) in the solid, as do **4** and **5** in the crystal [10]. The solid state EPR spectrum of **7** is distinct from the others and is clearly axial, with the $g_\parallel > g_\perp > g_e$ pattern and an $A_\parallel\{^{63,65}Cu\}$ value typical of a tetragonal $\{d_{x^2-y^2}\}^1$ or $\{d_{xy}\}^1$ Cu(II) species [27]. This is consistent with the crystal structure of this complex. The powder EPR spectrum of **3** is broad and unresolved.

The frozen solution EPR spectra of **6** and **8** in 10:1 MeCN:toluene and 10:1 $MeNO_2$:toluene are isotropic and uninformative. In contrast, **3**–**5** and **7** all exhibit axial or pseudo-axial frozen solution EPR spectra with $g_\parallel > g_\perp > g_e$, that are again consistent with $\{d_{x^2-y^2}\}^1$ or $\{d_{xy}\}^1$ Cu(II) species (Table 4) [27]. Hence, it seems clear that **3** and **7** both retain their crystallographic tetragonal geometry upon dissolution. However, there are some

Table 2
Selected bond lengths (Å) and angles (°) in the single crystal X-ray structures of $[Cu(OH_2)(L^1Me_2)](BF_4)_2$ (**3**), $[Cu(OH_2)_2(L^1Ph)](BF_4)_2$ (**4**) and $[CuCl(HOMe)(L^1Me_2)]BF_4$ (**7**)

3		**4**		**7**	
Bond lengths					
Cu(1)–N(2)	2.011(3)	Cu(1)–N(2)	2.1879(15)	Cu(1)–N(2)	2.063(3)
Cu(1)–N(10)	1.963(3)	Cu(1)–N(10)	1.9935(15)	Cu(1)–N(10)	2.025(3)
Cu(1)–N(18)	1.974(3)	Cu(1)–N(22)	1.9987(16)	Cu(1)–N(18)	2.016(3)
Cu(1)–O(24)	1.958(3)	Cu(1)–O(32)	2.0194(16)	Cu(1)–Cl(24)	2.2573(10)
Cu(1)–F(26)	2.531(2)	Cu(1)–O(33)	2.0276(16)	Cu(1)–O(25)	2.362(3)
Cu(1)–F(34)	3.049(3)				
Bond angles					
N(2)–Cu(1)–N(10)	90.06(12)	N(2)–Cu(1)–N(10)	90.12(6)	N(2)–Cu(1)–N(10)	84.28(12)
N(2)–Cu(1)–N(18)	89.11(12)	N(2)–Cu(1)–N(22)	91.97(6)	N(2)–Cu(1)–N(18)	89.58(12)
N(2)–Cu(1)–O(24)	172.36(14)	N(2)–Cu(1)–O(32)	97.49(7)	N(2)–Cu(1)–Cl(24)	174.32(9)
N(2)–Cu(1)–F(26)	101.11(10)	N(2)–Cu(1)–O(33)	112.24(6)	N(2)–Cu(1)–O(25)	91.52(11)
N(2)–Cu(1)–F(34)	102.25(9)	N(10)–Cu(1)–N(22)	177.84(6)	N(10)–Cu(1)–N(18)	168.02(13)
N(10)–Cu(1)–N(18)	178.64(12)	N(10)–Cu(1)–O(32)	89.44(7)	N(10)–Cu(1)–Cl(24)	93.15(9)
N(10)–Cu(1)–O(24)	90.58(14)	N(10)–Cu(1)–O(33)	87.60(7)	N(10)–Cu(1)–O(25)	103.70(12)
N(10)–Cu(1)–F(26)	91.42(10)	N(22)–Cu(1)–O(32)	89.73(7)	N(18)–Cu(1)–Cl(24)	92.01(10)
N(10)–Cu(1)–F(34)	81.81(10)	N(22)–Cu(1)–O(33)	92.12(7)	N(18)–Cu(1)–O(25)	86.70(12)
N(18)–Cu(1)–O(24)	90.10(14)	O(32)–Cu(1)–O(33)	150.12(7)	Cl(24)–Cu(1)–O(25)	94.02(8)
N(18)–Cu(1)–F(26)	89.80(10)				
N(18)–Cu(1)–F(34)	97.31(10)				
O(24)–Cu(1)–F(26)	86.49(12)				
O(24)–Cu(1)–F(34)	70.32(11)				
F(26)–Cu(1)–F(34)	155.65(7)				

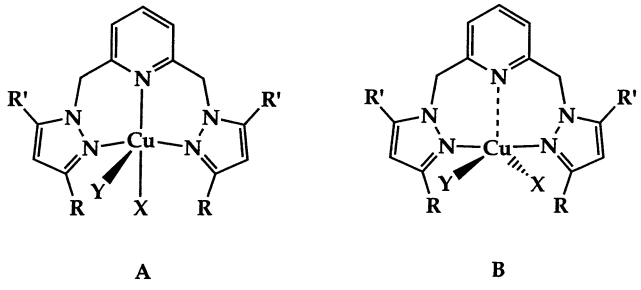

Scheme 2. Coordination geometries exhibited by $[CuXY(L^1R)]^{n+}$ complexes.

differences between the EPR spectra of **4** and **5** in these two phases. Therefore, the detailed stereochemistries of **4**–**6** and **8** in solution are presently uncertain. Importantly, for all complexes where the comparison could be made, these spectra are essentially invariant between solvents, suggesting that changing the identity of solvent ligands to the $[CuCl_x(solv)_{2-x}(L^1R)]^{(2-x)+}$ $(x = 0–2)$ centres barely perturbs the coordination geometry at Cu.

2.4. Electrochemistry

A preliminary voltammetric study was carried out in MeCN/0.1 M $NBu^n_4PF_6$ at 293 K, to elucidate the potentials of the $[Cu(solv)_xL]^{2+}/[Cu(solv)_yL]^{+}$ (L = L^1Me_2, L^1Ph) couples. Cyclic voltammograms (CVs)

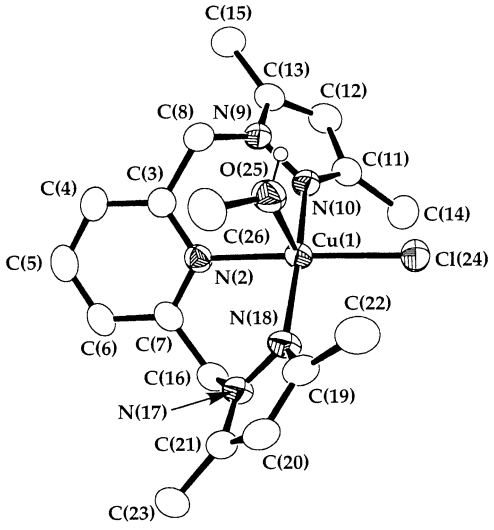

Fig. 5. View of the $[CuCl(HOMe)(L^1Me_2)]^{+}$ complex cation in the structure of **7**, showing the atom numbering scheme employed. Details as for Fig. 1.

of Cu(II) and Cu(I) complexes containing each ligand were run for comparison; in each case, the CVs obtained from the oxidised and reduced congeners of a given couple showed only small differences (Table 5).

For each Cu(II) complex **3** and **4**, a chemically reversible Cu(II/I) couple was obtained. However, plots of Ip versus $v^{1/2}$ (v = scan rate) for these processes did not give a straight line, showing that these couples are

Table 3
Conductivity and UV–Vis spectroscopic data for the Cu(II) compounds in this study (293 K)

	Solvent	Λ_M, Ω^{-1} cm^2 mol^{-1}	λ_{max}, nm (ε_{max}, M^{-1} cm^{-1})
$[Cu(OH_2)(L^1Me_2)](BF_4)_2\cdot H_2O$ (**3**·H_2O)	MeCN	219	260 (6,000), 319 (sh), 645 (69)
	$MeNO_2$	132	612 (70)
$[Cu(OH_2)_2(L^1Ph)](BF_4)_2$ (**4**)	MeCN	207	254 (39,000), 329 (2,200), 458 (280), 802 (70)
	$MeNO_2$	142	689 (70)
$[CuCl_2(L^1Me_2)]$ (**5**)	MeCN	8	267 (6,100), 345 (1,200), 768 (180)
	$MeNO_2$	6	766 (170)
$[CuCl_2(L^1Ph)]$ (**6**)	MeCN	13	254 (87,000), 343 (sh), 453 (150), 807 (139)
	$MeNO_2$	8	808 (135)
$[CuCl(HOMe)(L^1Me_2)]BF_4$ (**7**)	MeCN	128	268 (6,800), 340 (560), 692 (80)
	$MeNO_2$	79	688 (83)
$[CuCl(OH_2)(L^1Ph)]BF_4$ (**8**)	MeCN	112	248 (34,600), 332 (2,800), 413 (sh), 752 (142)
	$MeNO_2$	64	739 (145)

Table 4
X-band EPR data for the Cu(II) complexes in this study

		g_1	g_2	g_3	A_1
$[Cu(OH_2)(L^1Me_2)](BF_4)_2\cdot H_2O$ (**3**·H_2O)	Powder	2.07			
	MeCN	2.28	2.07	2.07	174
	$MeNO_2$	2.26	2.07	2.07	184
$[Cu(OH_2)_2(L^1Ph)](BF_4)_2$ (**4**)	Powder	2.30	2.15	2.04	
	MeCN	2.33	2.12	2.12	144
	$MeNO_2$	2.31	2.13	2.13	143
$[CuCl_2(L^1Me_2)]$ (**5**)	Powder	2.26	2.10	2.03	
	MeCN	2.29	2.10	2.10	161
	$MeNO_2$		2.12		
$[CuCl_2(L^1Ph)]$ (**6**)	Powder	2.28	2.09	2.04	
	MeCN		2.14		
	$MeNO_2$		2.14		
$[CuCl(HOMe)(L^1Me_2)]BF_4$ (**7**)	Powder	2.26	2.06	2.06	170
	MeCN	2.27	2.08	2.08	166
	$MeNO_2$	2.27	2.08	2.08	172
$[CuCl(OH_2)(L^1Ph)]BF_4$ (**8**)	Powder	2.28	2.10	2.04	
	MeCN		2.14		
	$MeNO_2$		2.14		

All spectra were obtained at 120 K. Hyperfine couplings are to ^{63,65}Cu and are in G. All solution spectra were run in solvents containing 10% toluene to aid glassing. Spectra with only one g value quoted are isotropic.

not electrochemically reversible. This probably reflects the kinetics of solvent coordination or decoordination that take place following Cu-based redox at these centres. The **1/3** couple is approximately 0.6 V more positive than the Cu(II/I) reduction previously reported for **5** in dmf [9], consistent with the presence of more strongly donating Cl^- coligands in the latter compound. Interestingly, the **2/4** couple is approximately +0.15 V more positive than the **1/3** couple, showing that the identity of the L^1R 'R' substituents has a substantial effect on the redox chemistry of the coordinated Cu ion.

3. Concluding remarks

Within the $[Cu(solv)_x(L^1R)]^{2+}/[Cu(solv)_y(L^1R)]^+$ system there are substantial structural variations, which appear to depend upon the identity of both 'R' and the exogenous ligands 'solv'. For the Cu(I) complexes, the ability of a $[Cu(L^1R)]^+$ fragment to bind exogenous ligands is dependent on the identity of 'R'. This is

Table 5
Cyclic voltammetric data for the complexes in this study (MeCN/0.1 M $NBu^n_4BF_4$, 298 K, $\nu = 100$ mV s^{-1})

	$E_{1/2}$ {Cu(II/I)} (V) (ΔEp, mV)	Epc{Cu(I/0)} (V)
$[Cu(NCMe)(L^1Me_2)]BF_4$ (**1**)	+0.14 (220)	−1.18
$[Cu(L^1Ph)]BF_4$ (**2**)	+0.29 (88)	−0.91
$[Cu(OH_2)(L^1Me_2)](BF_4)_2\cdot H_2O$ (**3**·H_2O)	+0.18 (244)	−1.20
$[Cu(OH_2)_2(L^1Ph)](BF_4)_2$ (**4**)	+0.33 (146)	−0.89

All potentials quoted vs. an internal ferrocene/ferrocenium standard.

presumably a steric effect, since the greater basicity of 3,5-dimethylpyrazole compared with 3{5}-phenylpyrazole [28] suggests that the $[Cu(L^1Ph)]^+$ moiety should be *less* electron-rich [29], and so more likely to bind exogenous ligands, than $[Cu(L^1Me_2)]^+$. This being the case, it is uncertain whether the lower oxidation potential of **1** compared with **2** is driven by the more donating character of L^1Me_2 compared with L^1Ph [29], or by the higher co-ordination number at Cu in **1**.

Combining our results with earlier work (Table 4), it is clear that $[Cu(II)XY(L^1R)]^{n+}$ (X, Y = halide, pseudohalide or solvent, $n = 0$–2) complexes can adopt one of two limiting geometries; tetragonal, with Y apical (structure A in Scheme 2); or, tetragonal with the L^1R pyridyl group apical (structure B). The available data suggest that these structural types can be distinguished by EPR spectroscopy (Table 6). All structurally authenticated type A complexes exhibit axial $g_\parallel > g_\perp \approx 2.07$ powder EPR spectra, where these can be clearly resolved, while all known type B complexes show strongly rhombic powder EPR spectra, with $g_3 \leq 2.04$. Bulky L^1R 'R' substituents appear to favour structure B, since EPR data show that all of the L^1Ph-containing complexes in this work exhibit structure B in the solid. Most of the L^1Me_2 complexes follow the trend expected on steric grounds, in that $[CuXY(L^1Me_2)]$ (X = Y = Cl, Br) adopt structure B while those complexes containing smaller N- or O-donor X and Y ligands exhibit structure A. However, the anomalous observation that $[Cu(N_3)_2(L^1Me_2)]$ is a structure B complex [9,12] suggests that electronic, as well as steric, factors might play a role in the stereochemistry of Cu(II)–L^1R complexes.

4. Experimental

Unless stated otherwise, all manipulations were performed in air using commercial grade solvents. 2,6-Bis-(chloromethyl)pyridine [20], 3-phenylpyrazole [19], L^1Me_2 [18], $[Cu(NCCH_3)_4]BF_4$ [30] and $[CuCl_2(L^1Me_2)]$ (**5**) [9,10] were prepared by the literature procedures. $Cu(BF_4)_2{\cdot}6H_2O$ (Avocado), KH (Aldrich) and all solvents were used as supplied, except that diglyme was dried over sodium before use. Microanalytical, mass spectrometric, UV–Vis, EPR and conductivity data for the complexes are listed in Tables 3, 4 and 7.

4.1. Synthesis of 2,6-bis-({3-phenylpyrazol-1-yl}methyl)pyridine (L^1Ph)

A mixture of 3-phenylpyrazole (15.9 g, 0.11 mol) and NaH (4.0 g, 0.11 M) in dry THF (50 cm^3) was stirred at 60 °C under N_2 for 30 min. 2,6-Bis-(chloromethyl)pyridine (9.7 g, 0.055 mol) was then added, and the mixture stirred at 60 °C for 24 h. The solvent was removed under reduced pressure and the residue taken up in chloroform (3×50 cm^3). The combined organic fractions were washed with water and saturated aqueous NaCl, then dried over $MgSO_4$. The filtered solution was evaporated to dryness to leave an off-white solid which was recrystallised from thf–Et_2O. Yield 15.0 g, 70% (Found: C, 76.7; H, 5.3; N, 18.1; Calc. for $C_{25}H_{21}N_5$: C, 76.4; H, 5.4; N, 17.8%). M.p. 98–100 °C. EI mass spectrum: m/z 391 $[M]^+$, 248 $[M-pz^{Ph}]^+$, 157 $[CH_2pz^{Ph}]^+$, 144 $[Hpz^{Ph}]^+$, 77 $[C_5H_3N]^+$. NMR spectra ($\{CD_3\}_2SO$, 293 K): ^1H; δ 7.93 (d, 2.3 Hz, 2H, Pz H^5), 7.77 (m, 5H, Ph $H^{2/6}$+Py H^4), 7.38 (m, 6H, Ph $H^{3/5}$+Ph H^4), 6.98 (d, 7.8 Hz, 2H, Py $H^{3/5}$), 6.78 (d, 2.3 Hz,

Table 6
Structural types and powder EPR spectra exhibited by crystallographically characterised Cu(II) 2,6-bis(pyrazolyl-1-ylmethyl)pyridine complexes

	Structure type [a]	τ [b]	g_1	g_2	g_3	Reference
$[Cu(OH_2)(L^1Me_2)](BF_4)_2$ (**3**)	A	0.10		2.07 [c]		This work
$[Cu(ONO_2)_2(L^1Me_2)]$	A	0.10		2.067 [c]		[10]
$[CuCl(HOMe)(L^1Me_2)]BF_4$ (**7**)	A	0.11	2.26	2.06	2.06	This work
$[Cu(ONO)(OClO_3)(L^1Me_2)]$	A	0.13	2.200	2.078	2.078	[12]
$[Cu(L^{10})(L^1Me_2)](ClO_4)_2$ [d]	A	0.14		2.076 [c]		[9]
$[Cu(NCS)_2(L^1Me_2)]$	A	0.26	2.258	2.085	2.085	[10,11]
$[CuBr_2(L^1Me_2)]$	B	0.14	2.236	2.105	2.041	[10]
$[CuCl_2(L^1Me_2)]$	B	0.16	2.252	2.092	2.027	This work, [10]
$[Cu(N_3)_2(L^1Me_2)]$	B	0.37	2.236	2.105	2.041	[9,12]
$[Cu(OH_2)_2(L^1Ph)](BF_4)_2$ (**4**)	B	0.46	2.30	2.15	2.04	This work
$[Cu(NCS)_2(L^{11})]$ [d]	B	0.45		[e]		[20]

[a] Scheme 2.
[b] Ref. [23].
[c] Broad, apparently isotropic spectrum.
[d] Scheme 1.
[e] Not reported.

Table 7
Analytical and selected FAB mass spectrometric data for the complexes in this study

		Found (Calc.)			
	Colour	%C	%H	%N	*m/z*
$[Cu(NCMe)(L^1Me_2)]BF_4$ (**1**)	Yellow	46.8 (46.9)	5.1 (5.0)	17.6 (17.3)	358
$[Cu(L^1Ph)]BF_4$ (**2**)	Pale yellow	55.3 (55.4)	3.9 (3.9)	13.2 (12.9)	454
$[Cu(OH_2)(L^1Me_2)](BF_4)_2\cdot H_2O$ (**3**·H_2O)	Blue	35.7 (35.9)	4.2 (4.4)	12.6 (12.3)	377, 358
$[Cu(OH_2)_2(L^1Ph)](BF_4)_2$ (**4**)	Red-brown	45.0 (45.2)	3.7 (3.8)	10.5 (10.5)	473, 454
$[CuCl_2(L^1Me_2)]$ (**5**)	Green	47.3 (47.5)	4.9 (4.9)	16.5 (16.3)	393, 358
$[CuCl_2(L^1Ph)]$ (**6**)	Green	56.0 (56.9)	3.9 (4.0)	13.5 (13.3)	489, 454
$[CuCl(HOMe)(L^1Me_2)]BF_4$ (**7**)	Blue	42.1 (42.1)	4.8 (4.9)	14.3 (13.6)	393, 358
$[CuCl(OH_2)(L^1Ph)]BF_4$ (**8**)	Brown	50.6 (50.4)	4.1 (3.9)	11.7 (11.8)	489, 454

2H, Pz H^4), 5.50 (s, 4H, CH_2). ^{13}C; δ 157.4 (Py $C^{2/6}$), 151.1 (Pz C^3), 138.0 (Py C^4+Pz C^5), 133.9 (Ph C^1), 129.7 (Ph $C^{2/6}$), 127.2 (Ph $C^{3/5}$), 125.0 (Ph C^4), 120.7 (Py $C^{3/5}$), 103.3 (Pz C^4), 57.6 (CH_2).

4.2. Synthesis of acetonitrile[2,6-bis-({3,5-dimethylpyrazol-1-yl}methyl)pyridine]copper(I) tetrafluoroborate (*1*)

A solution of L^1Me_2 (0.25 g, 8.4×10^{-4} mol) and $[Cu(NCMe)_4]BF_4$ (0.26 g, 8.4×10^{-4} mol) in MeCN (25 cm^3) was stirred under N_2 for 10 min at room temperature (r.t.). The yellow solution was concentrated to approximately 5 cm^3 and layered with Et_2O, affording a mixture of pale yellow needles and colourless blocks that were separated manually for analysis. The colourless crystals were identified as $[Cu(NCMe)_4]BF_4$ by comparison with a genuine sample. Yield of yellow crystals that were sufficiently large to separate by hand 0.064 g, 8%. IR spectrum (Nujol): 2310w, 2275w cm^{-1}.

4.3. Synthesis of [2,6-bis-({3-phenylpyrazol-1-yl}methyl)pyridine]copper(I) tetrafluoroborate (*2*)

A solution of L^1Ph (0.25 g, 6.4×10^{-4} mol) and $[Cu(NCMe)_4]BF_4$ (0.20 g, 6.4×10^{-4} mol) in $MeNO_2$ (25 cm^3) was stirred under N_2 for 10 min at r.t. The yellow solution was concentrated to approximately 5 cm^3 and layered with Et_2O, affording pale yellow needles. Yield 0.16 g, 47%.

4.4. Synthesis of [2,6-bis-({3,5-dimethylpyrazol-1-yl}methyl)pyridine]aquacopper(II) ditetrafluoroborate (*3*)

A solution of L^1Me_2 (0.25 g, 8.4×10^{-4} mol) and $Cu(BF_4)_2\cdot6H_2O$ (0.29 g, 8.4×10^{-4} mol) in $MeNO_2$ (25 cm^3) was stirred for 15 min at r.t. The resultant blue solution was concentrated to approximately 5 cm^3 and filtered. Vapour diffusion of Et_2O into this solution gave a sticky blue solid, which was dried over P_2O_5 and recrystallised from $MeNO_2$–Et_2O to give very hygroscopic blue blocks. Yield 0.29 g, 61%.

4.5. Synthesis of [2,6-bis-({3-phenylpyrazol-1-yl}methyl)pyridine]diaquacopper(II) ditetrafluoroborate (*4*)

A mixture of L^1Ph (0.25 g, 6.4×10^{-4} mol) and $Cu(BF_4)_2\cdot6H_2O$ (0.22 g, 6.4×10^{-4} mol) in $MeNO_2$ (25 cm^3) was stirred for 15 min at r.t., affording a green solution which was concentrated to approximately 5 cm^3 and filtered. Vapour diffusion of Et_2O into this solution yielded red–brown cubes. Yield 0.31 g, 73%.

4.6. Synthesis of dichloro[2,6-bis-({3-phenylpyrazol-1-yl}methyl)pyridine]copper(II) (*6*)

A suspension of L^1Ph (0.66 g, 1.7×10^{-3} mol) and $CuCl_2$ (0.22 g, 1.7×10^{-3} mol) in MeCN (30 cm^3) was stirred for 1 h at r.t., affording a green precipitate. This was filtered, washed with MeCN and Et_2O, and dried in vacuo. This product was analysed without further purification. Yield 0.58 g, 65%.

4.7. Synthesis of chloro[2,6-bis-({3,5-dimethylpyrazol-1-yl}methyl)pyridine](methanol)copper(II) tetrafluoroborate (*7*)

A solution of **5** (0.36 g, 8.4×10^{-4} mol) and $AgBF_4$ (0.16 g, 8.4×10^{-4} mol) in MeCN (25 cm^3) was stirred for 2 h at r.t. The blue solution was filtered, and evaporated to dryness. Recrystallisation of the residue from MeOH–Et_2O yielded dark blue microcrystals. Yield 0.17 g, 40%.

4.8. Synthesis of chloro[2,6-bis-({3-phenylpyrazol-1-yl}methyl)pyridine]aquacopper(II) tetrafluoroborate (*8*)

Method as for **7**, using **6** (0.44 g, 8.4×10^{-4} mol). The product formed green microcrystals from MeOH–Et_2O, which became brown upon drying. Yield 0.16 g, 52%.

4.9. Single crystal X-ray structure determinations

Single crystals of X-ray quality of [Cu(NCMe)-(L^1Me_2)]BF_4 (**1**) were grown by diffusion of ether into a solution of the complex in MeCN. Crystals of [Cu(L^1Ph)]BF_4 (**2**) and [Cu(OH_2)$_2$(L^1Ph)]$(BF_4)_2$ (**4**) were similarly grown from $MeNO_2$–Et_2O, and of [Cu(OH_2)(L^1Me_2)]BF_4 (**3**) and [CuCl(HOMe)(L^1Me_2)]-BF_4 (**7**) from MeOH–Et_2O. Experimental details from the structure determinations are given in Table 8. All structures were solved by direct methods (SHELXS-97 [31]) and refined by full-matrix least-squares on F^2 (SHELXL-97 [32]), with H atoms placed in calculated positions.

4.10. X-ray structure determinations of [Cu(NCMe)(L^1Me_2)]BF_4 (*1*) and [Cu(L^1Ph)]BF_4 (*2*)

No disorder was detected during the refinement of either of these structures, and no restraints were applied. All non-H atoms were refined anisotropically, and all H atoms were placed in calculated positions and refined using a riding model.

4.11. X-ray structure determination of [Cu(OH_2)(L^1Me_2)]$(BF_4)_2$ (*3*)

During refinement, one BF_4^- anion was found to be disordered by rotation about one B–F bond. The disordered F atoms were modelled over two equally occupied orientations. No restraints were applied. All non-H atoms with occupancy >0.5 were refined anisotropically. The H atoms for the aqua ligand were located in the difference map and allowed to refine freely; all other H atoms were placed in calculated positions and refined using a riding model.

4.12. X-ray structure determination of [Cu(OH_2)$_2$(L^1Ph)]$(BF_4)_2$ (*4*)

During refinement, one BF_4^- anion was found to be disordered over three orientations, with occupancy 0.50, 0.30 and 0.20. All B–F distances in the disordered anion were restrained to 1.38(2) Å, and non-bonded F···F distances within a given disorder orientation to 2.25(2) Å. All non-H atoms with occupancy ≥ 0.5 were refined anisotropically. The H atoms for the aqua ligands were located in the difference map and allowed to refine freely; all other H atoms were placed in calculated positions and refined using a riding model.

4.13. X-ray structure determination of [CuCl($HOCH_3$)(L^1Me_2)]BF_4 (*7*)

During refinement, the BF_4^- anion was found to be disordered over three equally occupied orientations. All B–F distances were restrained to 1.36(2) Å, and non-bonded F···F distances within a given disorder orientation to 2.22(2) Å. All wholly occupied non-H atoms were refined anisotropically. The hydroxyl H atom of the methanol ligand was located in the difference map and allowed to refine freely; all other H atoms were placed in calculated positions and refined using a riding model.

4.14. Other measurements

Infra-red spectra were obtained as Nujol mulls pressed between KBr windows, between 400 and 4000 cm^{-1} using a Nicolet Avatar 360 spectrophotometers. UV–Vis spectra were obtained with a Perkin–Elmer Lambda 900 spectrophotometer, operating between 1100 and 200 nm, in 1 cm quartz cells. All NMR spectra were run on a Bruker ARX250 spectrometer, operating at 250.1 MHz (^{1}H) and 62.9 MHz (^{13}C). Electron impact (EI) and positive ion fast atom bombardment (FAB) mass spectra were performed on a VG AutoSpec spectrometer, the FAB spectra employing a 3-NOBA matrix. CHN microanalyses were performed by the University of Leeds School of Chemistry microanalytical service. Melting points are uncorrected. X-band EPR spectra were obtained using a Bruker ER200D spectrometer.

Conductivity measurements were obtained with a Jenway 4310 analyser, at concentrations of approximately 5×10^{-3} mol dm^{-3}. All electrochemical measurements were carried out using an Autolab PGSTAT30 voltammetric analyser, in MeCN containing 0.1 M $NBu^n_4BF_4$ as supporting electrolyte. Cyclic voltammetric experiments involved the use of platinum working and counter electrodes and a silver wire reference electrode; all potentials quoted are referenced to an internal ferrocene/ferrocenium standard and were obtained at a scan rate of 100 mV s^{-1}.

5. Supplementary material

Full crystallographic data for the structure analyses in this study are available on request from the Cambridge Crystallographic Data Centre, 12 Union Road, Cambridge CB2 1EZ, UK (fax: +44-1223-336033; e-mail: deposit@ccdc.cam.ac.uk or www: http://www.ccdc.cam.ac.uk). The CCDC deposition numbers are 165783 (**1**), 165785 (**2**), 165786 (**3**), 165787 (**4**) and 165788 (**7**).

Table 8
Experimental details for the single crystal structure determinations in this study

	[Cu(NCMe)(L^{1}Me$_2$)]BF$_4$ (**1**)	[Cu(L^{1}Ph)]BF$_4$ (**2**)	[Cu(OH$_2$)(L^{1}Me$_2$)](BF$_4$)$_2$ (**3**)
Formula	$C_{19}H_{24}BCuF_4N_6$	$C_{25}H_{21}BCuF_4N_5$	$C_{17}H_{23}B_2CuF_8N_5O$
M_r	486.79	541.82	550.56
Crystal size (mm)	0.66 × 0.45 × 0.12	0.27 × 0.12 × 0.12	0.39 × 0.30 × 0.24
Crystal class	monoclinic	orthorhombic	monoclinic
Space group	$P2_1/c$	$P2_12_12_1$	$P2_1/c$
a (Å)	15.1864(2)	8.0834(2)	13.9278(4)
b (Å)	7.6452(1)	13.6690(3)	10.8144(4)
c (Å)	23.7158(3)	21.1714(5)	19.4236(6)
α (°)			
β (°)	129.4710(5)	–	129.485(2)
γ (°)			
V (Å^3)	2125.53(5)	2339.27(10)	2257.95(14)
Z	4	4	4
μ (Mo Kα) (mm^{-1})	1.081	0.990	1.053
T (K)		150(2)	
Diffractometer		Nonius KappaCCD area-detector	
Radiation, λ (Å)		Graphite-monochromated Mo Kα, 0.71073	
Measured reflections	81608	34397	20524
Independent reflections	4871	5328	4963
R_{int}	0.060	0.066	0.071
Absorption correction		Multi-scan	
Min. transmission	0.54	0.78	0.68
Max. transmission	0.88	0.89	0.79
Observed reflections [$I > 2\sigma(I)$]	4457	4642	4066
Range in 2θ (°)	$3.4 \le 2\theta \le 55.1$	$3.8 \le 2\theta \le 54.9$	$7.7 \le 2\theta \le 55.0$
Range in h	$-19 \le h \le 19$	$-10 \le h \le 10$	$-18 \le h \le 18$
Range in k	$-9 \le k \le 9$	$-17 \le k \le 17$	$-14 \le k \le 13$
Range in l	$-30 \le l \le 30$	$-27 \le l \le 27$	$-25 \le k \le 25$
Parameters/restraints	289/0	326/0	333/0
$R(F)$ [a], $wR(F^2)$ [b]	0.029, 0.080	0.035, 0.078	0.063, 0.166
Goodness-of-fit	1.047	1.031	1.078
Weighting scheme [c]	$w = 1/[\sigma^2(F_o^2)+(0.0397P)^2+1.0105P]$	$w = 1/[\sigma^2(F_o^2)+(0.0381P)^2+0.4381P]$	$w = 1/[\sigma^2(F_o^2)+(0.0352P)^2+0.6207P]$
$\Delta\rho$ (max/min) (e Å^{-3})	0.37/−0.58	0.34/−0.42	0.60/−0.73
Flack parameter	–	−0.009(10)	–

	[Cu(OH$_2$)$_2$(L^{1}Ph)](BF$_4$)$_2$ (**4**)	[CuCl(HOMe)(L^{1}Me$_2$)]BF$_4$ (**7**)
Formula	$C_{25}H_{25}B_2CuF_8N_5O_2$	$C_{18}H_{25}BClCuF_4N_5O$
M_r	664.66	513.23
Crystal size (mm)	0.30 × 0.24 × 0.24	0.51 × 0.30 × 0.18
Crystal class	monoclinic	triclinic
Space group	$P2_1/c$	$P\bar{1}$
a (Å)	18.3780 (3)	10.2687(1)
b (Å)	8.9210(2)	10.9259(1)
c (Å)	16.5700(3)	11.9993(2)
α (°)		89.531(1)
β (°)	94.037(1)	64.997(1)
γ (°)		70.373(1)
V (Å^3)	2709.91(9)	1135.01(2)
Z	4	2
μ (Mo Kα) (mm^{-1})	0.896	1.132
T (K)		150(2)
Diffractometer		Nonius KappaCCD area-detector
Radiation, λ (Å)		Graphite-monochromated Mo Kα, 0.71073
Measured reflections	45581	44356
Independent reflections	6179	5060
R_{int}	0.042	0.151
Absorption correction	Multi-scan	
Min. transmission	0.77	0.60

Table 8 (*Continued*)

	$[Cu(OH_2)_2(L^1Ph)](BF_4)_2$ (**4**)	$[CuCl(HOMe)(L^1Me_2)]BF_4$ (**7**)
Max. transmission	0.81	0.82
Observed reflections $[I > 2\sigma(I)]$	5257	4591
Range in 2θ (°)	$4.4 \le 2\theta \le 55.0$	$3.8 \le 2\theta \le 55.1$
Range in h	$-23 \le h \le 23$	$-13 \le h \le 13$
Range in k	$-11 \le k \le 11$	$-14 \le k \le 14$
Range in l	$-20 \le l \le 21$	$-15 \le l \le 15$
Parameters/restraints	467/30	301/30
$R(F)$ [a], $wR(F^2)$ [b]	0.037, 0.099	0.068, 0.170
Goodness-of-fit	1.024	1.069
Weighting scheme [c]	$w = 1/[\sigma^2(F_o^2)+(0.0517P)^2+1.6824P]$	$w = 1/[\sigma^2(F_o^2)+(0.0746P)^2+1.1726P]$
$\Delta\rho$ (max/min) (e Å^{-3})	0.44/−0.60	0.80/−0.85
Flack parameter		

[a] $R = \Sigma[|F_o|-|F_c|]/\Sigma|F_o|$.
[b] $wR = [\Sigma w(F_o^2-F_c^2)/\Sigma wF_o^4]^{1/2}$.
[c] $P = (F_o^2+2F_c^2)/3$.

Acknowledgements

The authors thank the Royal Society for a research fellowship to M.A.H., the EPSRC for a studentship to C.L.F., and the University of Leeds.

References

[1] N. Kitajima, W.B. Tolman, Prog. Inorg. Chem. 43 (1995) 419.
[2] W.B. Tolman, Acc. Chem. Res. 30 (1997) 227.
[3] K.D. Karlin, A.D. Zuberbühler, in: J. Reedijk, E. Bouwman (Eds.), Bioinorganic Catalysis, second ed., Marcel Dekker, New York, 1999, pp. 469–534.
[4] S. Schindler, Eur. J. Inorg. Chem. (2000) 2311.
[5] J.P. Klinman, Chem. Rev. 96 (1996) 2541.
[6] B.A. Averill, Chem. Rev. 96 (1996) 2951.
[7] E.I. Solomon, U.M. Sundaram, T.E. Machonkin, Chem. Rev. 96 (1996) 2563.
[8] B.J. Hathaway, in: G. Wilkinson, R.D. Gillard, J.A. McCleverty (Eds.), Comprehensive Coordination Chemistry, vol. 5, Pergamon, Oxford, 1987, pp. 596–619.
[9] T.K. Lal, R. Gupta, S. Mahapatra, R. Mukherjee, Polyhedron 18 (1999) 1743.
[10] P. Manikandan, K.R.J. Thomas, P.T. Manoharan, J. Chem. Soc., Dalton Trans. (2000) 2779.
[11] P. Manikandan, K.R.J. Thomas, P.T. Manoharan, Acta Crystallogr., Sect. C 56 (2000) 308.
[12] R. Gupta, R. Mukherjee, Polyhedron 20 (2001) 2545.
[13] (a) K.D. Karlin, M.S. Haka, R.W. Cruse, G.J. Meyer, A. Farooq, Y. Gultneh, J.C. Hayes, J. Zubieta, J. Am. Chem. Soc. 110 (1988) 1196;
(b) I. Blain, M. Giorgi, E. Lojou, D. Lexa, M. Réglier, Eur. J. Inorg. Chem. (1998) 1297;
(c) I. Blain, P. Bruno, M. Giorgi, I. De Riggi, M. Réglier, Eur. J. Inorg. Chem. (2000) 393.
[14] C. Piguet, B. Bocquet, E. Müller, A.F. Williams, Helv. Chim. Acta 72 (1989) 323.
[15] D.A. Evans, M.C. Kozlowski, J.A. Murry, C.S. Burgey, K.R. Campos, B.T. Connell, R.J. Staples, J. Am. Chem. Soc. 121 (1999) 669.
[16] (a) K. Bernauer, F. Gretillat, H. Stoeckli-Evans, R. Warmuth, Helv. Chim. Acta 76 (1993) 545;
(b) K. Bernauer, T. Chuard, H. Stoeckli-Evans, Helv. Chim. Acta 76 (1993) 2263.
[17] (a) C. Piguet, G. Bernardinelli, A.F. Williams, Inorg. Chem. 28 (1989) 2920;
(b) S. Rüttigman, C. Piguet, G. Bernardinelli, B. Bocquet, A.F. Williams, J. Am. Chem. Soc. 114 (1992) 4230;
(c) R.F. Carina, A.F. Williams, C. Piguet, Helv. Chim. Acta 81 (1998) 548.
[18] S. Mahapatra, N. Gupta, R. Mukherjee, J. Chem. Soc., Dalton Trans. (1991) 2911.
[19] S. Trofimenko, J.C. Calabrese, J.S. Thompson, Inorg. Chem. 26 (1987) 1507.
[20] W. Baker, K.M. Buggle, J.W.F. McOmie, D.A.M. Watkins, J. Chem. Soc. (1958) 3594.
[21] A.A. Watson, D.A. House, P.J. Steel, Inorg. Chim. Acta 130 (1987) 167.
[22] (a) P. Manikandan, B. Varghese, P.T. Manoharan, J. Chem. Soc., Dalton Trans. (1996) 371;
(b) P. Manikandan, M. Subramoni, B. Varghese, P.T. Manoharan, J. Chem. Soc., Dalton Trans. (1998) 3219.
[23] A.W. Addison, T.N. Rao, J. Reedijk, J. van Rijn, G.C. Verschoor, J. Chem. Soc., Dalton Trans. (1984) 1349.
[24] W.J. Geary, Coord. Chem. Rev. 7 (1971) 81.
[25] D.F. Shriver, P.W. Atkins, Inorganic Chemistry, third ed., Oxford University Press, Oxford, 1999, p. 228.
[26] See e.g. M. Lanfranchi, M.A. Pellinghelli, G. Predieri, F. Bigi, R. Maggi, G. Sartori, J. Chem. Soc., Dalton Trans. (1993) 1463.
[27] B.A. Goodman, J.B. Raynor, Adv. Inorg. Chem. 13 (1970) 135.
[28] J. Elguero, E. Gonzalez, R. Jacquier, Bull. Soc. Chim. Fr. (1968) 5009.
[29] J.M. Holland, C.A. Kilner, M. Thornton-Pett, M.A. Halcrow, Polyhedron 20 (2001) 2829.
[30] G.J. Kubas, Inorg. Synth. 28 (1990) 68.
[31] G.M. Sheldrick, Acta Crystallogr., Sect. A 46 (1990) 467.
[32] G.M. Sheldrick, SHELXL-97, Program for the refinement of crystal structures, University of Göttingen, 1997.